, Barnouin, O., Daly, M., Palmer, E., Gaskell, R., Weirich, J., Johnson, C., Al Asad, M., Roberts, J., Perry, M., Susorney, H., Daly, R., Bierhaus, E., Seabrook, J., Espiritu, R., Nair, A., Nguyen, L., Neumann, G., Ernst, C., ... Lauretta, D. (2019). Shape of (101955) Bennu indicative of a rubble pile with internal stiffness. *Nature Geoscience*, *12*(4), 247-252. https://doi.org/10.1038/s41561-019-0330-x

Exploring the shape of (101955) Bennu with OSIRIS-REx.

O.S. Barnouin[1], M.G. Daly[2], E.E Palmer[3], R.W. Gaskell[3], J.R. Weirich[3], C.L. Johnson[3,4], M.M. Al Asad[4], J.H. Roberts[1], H.C.M. Susorney[4], T. Daly[1], E.B. Bierhaus[5], J. Seabrook[3], M.E. Perry[1], R.M. Espiritu[1], A.H. Nair[1], L. Nguyen[1], G.A. Neumann[6], C.M. Ernst[1], W.V. Boynton[7], M.C. Nolan[7], C. Adam[8], M.C. Moreau[6], B. Risk[7], C. D'Aubigny[7], E.R. Jawin[9], K.J. Walsh[10], P. Michel[11], S.R. Schwartz[7], R.-L. Ballouz[7], D.N. DellaGiustina[7], E.M. Mazarico[6], D.J. Scheeres[12], J. McMahon[12], S. Sugita[13], N. Hirata[14], S. Watanabe[15] and D.S. Lauretta[7].

[1]The Johns Hopkins University Applied Physics Laboratory, Laurel, MD, USA (olivier.barnouin@jhuapl.edu).
[2]The Centre for Research in Earth and Space Science, York University, Toronto, Ontario, Canada.
[3]Planetary Science Institute, Tucson, AZ, USA.
[4]Department of Earth, Ocean and Atmospheric Sciences, University of British Columbia, Vancouver, Canada.
[5]Lockheed Martin Space Systems Company, Denver, CO, USA.
[6]NASA Goddard Space Flight Center, Greenbelt, MD, USA.
[7]Lunar Planetary Laboratory, University of Arizona, Tucson, AZ, USA.
[8]Smithsonian Institution National Museum of Natural History, Washington, DC, USA.
[9]KinetX Aerospace, Inc. Simi Valley, CA, USA.
[10]Southwest Research Institute, Boulder, CO, USA.
[11]Université Côte d'Azur, Observatoire de la Côte d'Azur, CNRS, Laboratoire Lagrange, Nice, France.
[12]Department of Aerospace Engineering Sciences, University of Colorado, Boulder, CO, USA.
[13]University of Tokyo, Tokyo, Japan.
[14]Aizu University, Aizu-Wakamatsu, Japan.
[15]Institute of Space and Astronautical Science, JAXA, Sagamihara, Japan.

Despite 4.5 billion years of evolution, some solar system asteroids have remained relatively pristine, preserving worlds that formed Earth and contributed to the early evolution of life. In November 2018, the OSIRIS-REx mission arrived at asteroid (101955) Bennu and began detailed observations of one of these small, primitive objects. Here we show that the global shape of Bennu reveals evidence of the asteroid's formation, internal structure, and dynamic history. The spinning top shape, volume and mass indicate that Bennu is a rubble pile. Its most prominent feature is a cratered equatorial ridge that formed early in its history. The presence of high-standing, north-south ridges, that extend from the

poles to the equator, and are not found on other asteroids may reflect internal stiffness. Surface mass movements indicate material that has flowed over a less-mobile interior. Together, these observations suggest that Bennu underwent an early history of enhanced spin, possibly reaching a state of near complete disruption to form the north-south ridges. Since then, the asteroid may have undergone intermittent periods of spin-up leading to moderate surficial modifications during its wanderings from the main belt to the inner solar system.

Asteroid (101955) Bennu, hereafter Bennu, was known, through radar and light-curve modelling [1], to have a fairly smooth ‘‘spinning top’’ shape with an equatorial ridge. The mean diameter was estimated to be 492 ± 20 m and the asteroid volume 0.0623 ± 0.006 km^3. A single boulder, 10 to 20 m across was apparent on a surface that was otherwise smooth at a resolution of 7.5 m. A rotation period of 4.29746 ± 0.002 hr was estimated, about an axis with a pole at (88°, -45°) ± 4° in ecliptic coordinates.

The Origins, Spectral Interpretation, Resource Identification, Security, Regolith Explorer (OSIRIS-REx) mission began collecting resolved images of asteroid (101955) Bennu in early November 2018 using the OSIRIS-REx camera suite (OCAMS) [2]. These images were used to develop a global shape model of the asteroid as the basis for most geophysical investigations of Bennu and for proximity spacecraft navigation. Stereophotoclinometry (SPC) [3], a well-established technique that merges stereo imaging with photoclinometry, was used to generate a shape model with a resolution of 0.8 m (Fig. 1). The model has a best-fit ellipsoid with dimensions (563.87 ± 0.17) x (536.09 ± 0.17) x (498.42 ± 0.17) m, a volume of 0.06157 ± 0.0007 km^3 and a surface area of 0.8232 ± 0.0009 km^2. Use of additional limb images and stereo data, as well as ranges measured by the OSIRIS-REx laser altimeter (OLA [4]; Fig. 1) provide validation of the average radius to 0.17 m (Fig. S1). The pole position and rotation period are given in Fig. 1, and the Prime Meridian is defined by Boulder H (S2). Pole wobble is constrained to be less than 0.2° and a small (< 2 m) centre-of-mass (COM) centre-of-figure (COF) offset is present, dominantly in the direction of the Prime Meridian.

By volume, Bennu is about three-and-half times larger than (25143) Itokawa [5] and about six times smaller than (162173) Ryugu [6]. Bennu is spectroscopically similar to CI and CM meteorites [7]. The mass estimate for Bennu 7.32 ± 0.003 x 10^{10} kg [8], which along with the average measured [9] bulk densities of CI and CM meteorites (density of 1570 to 2300 kg m^{-3}), yields macroporosity values ranging from 25% (CI) to 50% (CM) and corresponding total porosities of 60% to 70%. Typical cohesionless sand has a macro porosity of 35 to 45% [10], while Itokawa and Ryugu possess estimated total porosities of (44 ± 4)% [5] and more than 50% [6] respectively. The bulk density,

together with implications of the COM-COF offset for interior density distributions are discussed in [8].

The OSIRIS-REx observations confirm the Earth-based radar shape model [1] — Bennu is diamond or top-shaped, with an equatorial ridge (Fig. 1). OSIRIS-REx data however, show that the ridge is not uniform in elevation (Fig. 1), and is more muted relative to equatorial ridges on other small asteroids such as Ryugu [5] and KW4 [11].

Superposed on, and contributing to this global shape are a number of surface features (Fig. 2) including additional ridges, scarps, and troughs (lows with a distinct flat base). Additional features with measurable topography include craters, landslide deposits and boulders (the largest of which contribute to the shape of Bennu), as well as grooves (quasi-linear depressions without flat bottoms).

At least four major north-south ridges, hereafter referred to as longitudinal ridges, have been mapped in the northern hemisphere and two in the southern hemisphere (Figs. 2, 3). The largest boulder on Bennu, Boulder A [12], located in the southern hemisphere is part of one of these southern ridges. The peak-to-trough relief (i.e. top of the ridge to base of the low lying topography between the ridges) associated with the ridges is 2 - 5 m and ridge lengths can reach 400 m. Boulders are concentrated in the local topographic lows between these ridges [13].

Several scarps have also been identified in images and in the topography. The largest of the scarps is located in the northern hemisphere (Fig. 2d) and spans at least 120º of longitude at ~50°N. It has a ~5m wide ledge with a small slope of 10-15º, and a 3–6 m drop with near 40º to the north. There are additional shorter scarps with varying widths and heights seen above rock deposits in several locations across the mid-latitudes.

Candidate craters have been identified [13], the largest has a diameter (D) of 130 m. A geometric assessment of the depths (d) of a few of the largest, most-likely [13], candidate craters gives d/D ~ 0.13. Geopotential altitude, determined relative to a geoid, yields d/D ~ 0.18. Thus, these craters are similar to those on other larger asteroids (Eros, Lutetia, Vesta) for which d/D ~ 0.15 [14] and to 453 Mathilde (d/D = 0.12 to 0.25 [15]), the only other C-type asteroid for which crater depths have been published. However, they are deeper than the maximum of 0.1 reported for Itokawa [16]. Most of the best-preserved crater candidates appear to be preferentially located at low-latitudes (<30º) along the equatorial ridge [13].

Several aspects of Bennu's topography support the pre-arrival expectation [17] that Bennu is a rubble-pile asteroid. The size of Bennu's largest boulders, which approach

25 - 33% of the diameter of the largest identified crater candidate, are too large volumetrically to have been excavated from craters and deposited as ejecta [18]. Furthermore, the largest boulders control surface roughness over spatial scales of 10 m. The largest boulders are located on the -Z (southern) hemisphere (Fig. 2a) and are several 10s of m high and more 40 m in diameter. The large boulders are inferred to be remnants of Bennu's parent body, accreted after the event that destroyed it [19]. At 60% to 70%, Bennu's high total porosity is inconsistent with a monolithic body and may be the strongest evidence for a rubble pile interior. Scheeres et al. [8] report that density inhomogeneities that can be modeled in terms of few large boulders, consistent with a rubble pile structure, could explain Bennu's COM-COF offset.

Bennu's overall shape also has features that imply internal shear strength and/or cohesion to support the non-hydrostatic shape and the high-standing ridges. A hydrostatic shape (e.g., Maclaurin ellipsoid [20]) with Bennu's density and rotation rate is not stable, and Bennu must have a minimum internal friction angle, in the absence of cohesion, of at least 18 degrees to support the current shape (Fig. S1A). These properties are consistent with those of granular materials [10]. The long ridges also denote internal stiffness as they support material above surrounding terrain. Further evidence for interior strength are linear grooves (Fig. 2c) with widths of 10-15 m and depths of 2 - 3 m that span 50 to 100 m. Similar features were used as evidence for internal shear strength on 433 Eros [21].

The global contribution of the equatorial ridge and the longitudinal ridges to Bennu's shape is evident in a low degree spherical harmonic description of the shape model (Fig. 4). Furthermore, the shape has no substantial long-wavelength north-south hemispheric asymmetry (Figs. 1, 4). The longitudinal ridges, together with several large craters, result in pronounced deviations of the shape in the equatorial plane from a circle (Fig. 3). The equatorial signature of these ridges is approximately periodic in longitude with a wavelength of 90°, and accounts for ~33% of the power in the deviations from a circular shape.

The global shape model has evidence of several areas where loose surface material flowed (Fig. 2e). The best example is a landslide that infills one of the largest candidate craters, flowing over the western rim leaving a ~5m-thick deposit. Additional indications of mass movements are boulder concentrations at the base of long slopes, particularly between the high-standing ridges [13]. One candidate crater (near 40°N, 160°E), is almost completely buried, indicating activity that post-dated the crater formation.

Bennu's shape provides a window into the asteroid's formation and evolution processes. Several models for rotational evolution show that for asteroids with stiffer

interiors (resulting from packing of internal constituents, for example) are more likely to currently generate mass movements similar to those suggested by the observations [22, 23, 24]. This provides additional evidence for an underlying structure with strength, consistent with a few large fragments which anchor the rubble.

Bennu is susceptible to radiative-driven spin-up processes known as YORP [25]. Bennu's top-shape and equatorial ridge could have formed when Bennu was rotating faster either during re-accumulation [26] or by YORP. The well-preserved large craters on the equatorial ridge [13] suggests that the ridge is old, likely predating Bennu's exit from the main belt [13]. The formation of the ridge, usually easier to develop when the interior has lower cohesion [22, 23], might also indicate a time when Bennu's interior was weaker (lower friction angle and or cohesion) than the evidence for longitudinal ridges and surface flows suggest exist today.

An unexpected finding is that the YORP process acting since the formation of the early equatorial bulge has not subsequently accelerated Bennu (spin-up) sufficiently to reshape the ridge and erase the equatorial craters. Asteroids with surfaces that can be frequently refigured, to an extent that can interrupt spin acceleration, can lead to chaotic YORP. Evidence for surface modification, described above, may explain the stable ridge and is supported by the presence of steep slopes and modified craters at mid-to-high latitudes.

The current shape and surface of Bennu is consistent with stiffness and interior cohesion. Numerical investigations of the disruption of rubble piles due to spin-up [24] show that when cohesion is present (somewhere between 1-30Pa), the asteroid fails in tension, usually in well-defined wedges. The long-wavelength longitudinal structure of Bennu provides strong support for such a process.

References:

[1] Nolan, M. C, C. Magri, E. S Howell, L. A. M. Benner, J. D Giorgini, C. W. Hergenrother, and R. S. Hudson, 2013. "Shape model and surface properties of the OSIRIS-REx target Asteroid (101955) Bennu from radar and lightcurve observations." Icarus 226: 629–40. doi:0.1016/j.icarus.2013.05.028

[2] Rizk, B., C. Drouet d'Aubigny, D. Golish, C. Fellows, C. Merrill, P. Smith, M. S. Walker, 2018. "OCAMS: The OSIRIS-REx Camera Suite." Space Science Reviews 214 (1): 26. doi:10.1016/j.asr.2018.08.020.

[3] Gaskell, R W, O. S. Barnouin-Jha, D J Scheeres, A S Konopliv, T Mukai, S Abe, J Saito, 2008. “Characterizing and navigating small bodies with imaging data.” Meteoritics and Planetary Science 43 (6): 1049–61. doi:10.1111/j.1945-5100.2008.tb00692.x

[4] Daly, M G, O S Barnouin, C Dickinson, J Seabrook, C L Johnson, G Cunningham, T Haltigin, 2017. “The OSIRIS-REx Laser Altimeter (OLA) Investigation and Instrument.” Space Science Reviews 198 (1): 1–26. Doi: 10.1007/s11214-017-0375-3

[5] Abe, S., T. Mukai, N. Hirata, O. S. Barnouin-Jha, A.F. Cheng, H. Demura, R. W. Gaskell, T. Hashimoto, K. Hiraoka, T. Honda, T. Kubota, M. Matsuoka, T. Mizuno, R. Nakamura, D. J. Scheeres, and M. Yoshikawa, 2006. Mass and Local Topography Measurements of Itokawa by Hayabusa. Science 312(5778), pp.1344–1347. Doi: 10.1126/science.1126272

[6] Watanabe, S. M. Hirabayashi, N. Hirata, N. Hirata, R. Noguchi, Y. Shimaki, E. Tatsumi, M. Yoshikawa, S. Kikuchi, H. Yabuta, T. Nakamura, S. Tachibana, Y. Ishihara, T. Morota, K. Matsumoto, K. Wada, H. Senshu, C. Honda, T. Michikami,T. Kouyama, R. Honda, H. Takeuchi, S. Sugita, K. Kitazato, T. Okada, N. Namiki, H. Ikeda, R. Gaskell, E. Palmer, O. S. Barnouin, P. Michel,A. French, J. W. McMahon, D. J. Scheeres, P. A. Abell, Y. Yamamoto, S. Tanaka, K. Shirai, N. Sakatani, M. Matsuoka, S. Tanaka, M. Yamada, Y. Yokota, N. Nishikawa, T. Sugiyama, T. Yamaguchi, N. Ogawa, G. Ono, Y. Mimasu, K. Yoshikawa, T. Takahashi, Y. Takei, A. Fujii, M. Abe, M. Hayakawa, S. Hosoda, O. Mori, H. Sawada, T. Shimada, S. Soldini, H. Yano, M. Fujimoto, Y. Iijima, K. Ogawa, T.-M. Ho, A. Moussi, R. Jaumann, J.-P. Bibring, C. Krause, F. Terui, T. Saiki, S. Nakazawa, and Y. Tsuda (2019), Hayabusa2 observation of the top-shape carbonaceous asteroid 162173 Ryugu. Submitted to Science.

[7] Hamilton et al. (this issue)

[8] Scheeres et al. (this issue)

[9] R. J. Macke, G. J. Consolmagno, D.T. Britt, Density, porosity, and magnetic susceptibility of carbonaceous chondrites. Meteorit. Planet. Sci. 46, 1842-1862 (2011). doi: 10.1111/j.1945-5100.2011.01298.x

[10] Das, B. M. and Sivakugan, N. (2017). Fundamentals of Geotechnical Engineering, Cengage Learning, Boston, pp. 778.

[11] Ostro, S.J., J.-L. Margot, L. A. M. Benner, J. D. Giorgini, D. J. Scheeres, E. G. Fahnestock, S. B. Broschart, J. Bellerose, M. C. Nolan, C. Magri, P. Pravec, P.

Scheirich, R. Rose,R. F. Jurgens, E. M. De Jong, and S. Suzuki, 2006. Radar Imaging of Binary Near-Earth Asteroid (66391) 1999 KW4. Science, 314(5803), pp.1276–1280.

[12] Lauretta et al. this issue

[13] Walsh et al. this issue.

[14] Marchi, S., C. R. Chapman, O. S. Barnouin, J. E. Richardson and J-B Vincent, 2015. Cratering on Asteroids. In Asteroids IV. University of Arizona Press, pp. 725–744.

[15] Thomas, P.C., J. Vevreka, J.F. Bell, B.E. Clark, C. Brian, J. Joseph, M. Robinson, L.A. McFadden, M.C. Malin, C.R. Chapman, W. Merline and S. Murchie, 1999. Mathilde: Size, Shape, and Geology. Icarus, 140, p.17. Doi: 10.1006/icar.1999.6121

[16] Hirata, N. O. S. Barnouin-Jha, C.Honda, R. Nakamura, H. Miyamoto, S. Sasaki, H. Demura, A. M. Nakamura, T. Michikami, R. W. Gaskell, and J. Saito, 2009. A survey of possible impact structures on 25143 Itokawa. 200(2), pp.486–502.

[17] Michel, P., Willy Benz, Paolo Tanga, Derek C. Richardson, 2001. Collisions and Gravitational Reaccumulation: Forming Asteroid Families and Satellites. Science 294(5547), pp.1696–1700.

[18] Bart, G. D., and H. J. Melosh (2007), Using lunar boulders to distinguish primary from distant secondary impact craters, Geophys. Res. Lett., 34, L07203, doi:10.1029/2007GL029306.

[19] Michel, P. & Richardson, D.C., 2013. Collision and gravitational reaccumulation: possible formation mechanism of the asteroid Itokawa. Astronomy and Astrophysics, pp.1–4.

[20] Holsapple, K.A. 2004. Icarus 172, 272–303.

[21] Prockter, L., P. Thomas, M. Robinson, J. Joseph, A. Milne, B. Bussey, J. Veverka and A. Cheng, 2002. Surface Expressions of Structural Features on Eros. Icarus 155, pp.75–93.

[22] M. Hirabayashi, D. J. Scheeres, Stress and failure analysis of rapidly rotating asteroid (29075) 1950 DA. Astrophys J. Lett. 798, L8 (2014). doi: 10.1088/2041-8205/798/1/L8

[23] Zhang, Y., D. C. Richardson, O. S. Barnouin, C. Maurel, P. Michel, S. R. Schwartz, R.-L. Ballouz, L. A.M. Benner, S. P. Naidu, and J. Libe, 2017. Creep stability of the proposed AIDA mission target 65803 Didymos: I. Discrete cohesionless granular physics model. 294, pp.98–123. doi:10.1016/j.icarus.2017.04.027

[24] Y. Zhang, D. C. Richardson, O. S. Barnouin, P. Michel, S. R. Schwartz, R.-L. Ballouz, Rotational failure of rubble-pile bodies: influences of shear and cohesive strengths. Astrophys. J. 857, 15 (2018). doi: 10.3847/1538-4357/aab5b2

[25] Rubincam, D.P., 2000. Radiative Spin-up and Spin-down of Small Asteroids. Icarus, 148(1), pp.2–11.

[26] Michel, P., O. Barnouin, R.L. Ballouz, K. Walsh, D.C. Richardson, S. R. Schwartz, M. Jutzi, S. Sugita, S. Watanabe, M. Hirabayashi, H. Miyamoto, W.F. Bottke Jr., H.C. Connolly Jr., D. S. Lauretta and the Hayabusa 2 and OSIRIS-REx teams, Disruption and reaccumulation as the possible origins,

Figures:

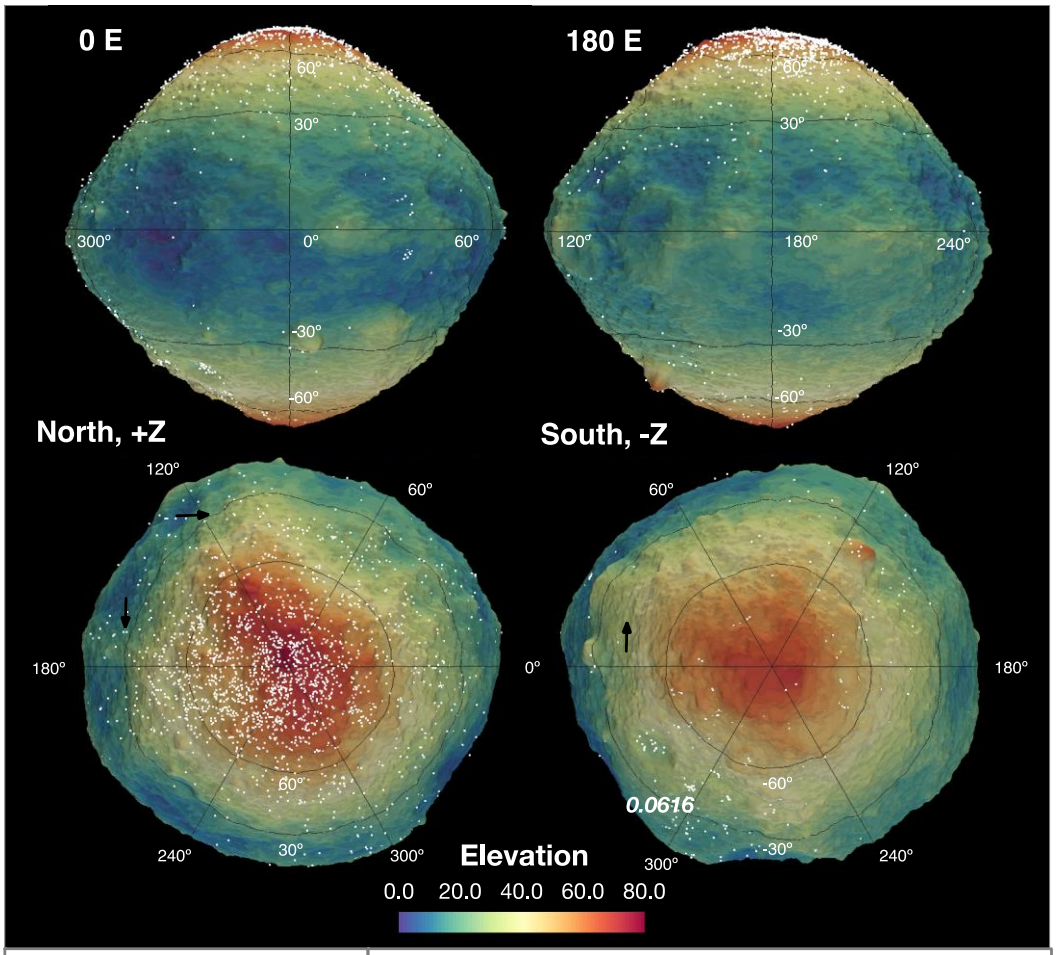

Parameter	Value
Extent	(563.87 ± 0.17)x(536.09 ± 0.17)x(498.42 ± 0.17)
Volume	0.06157 ± 0.0007 km^3
Surface Area	0.8232 ± 0.0009 km^2
Pole	RA = (85.34 ± 0.2)° DEC =(-60.15 ± 0.2)°
Period	4.29605858 hrs + (1.73611x10^{-10})t t = time in hours in J2000 epoch
Center of Mass / Center of Figure Offset	[1.4, -0.5, -0.15] ±0.17 m

Figure 1: The Global digital terrain model of Bennu. OLA footprint locations are overlain (white spots) and table of model parameters is shown (bottom right). The upper panels show geopotential altitude or elevation above a reference geoid. Arrows indicate location of prominent NS-ridges.

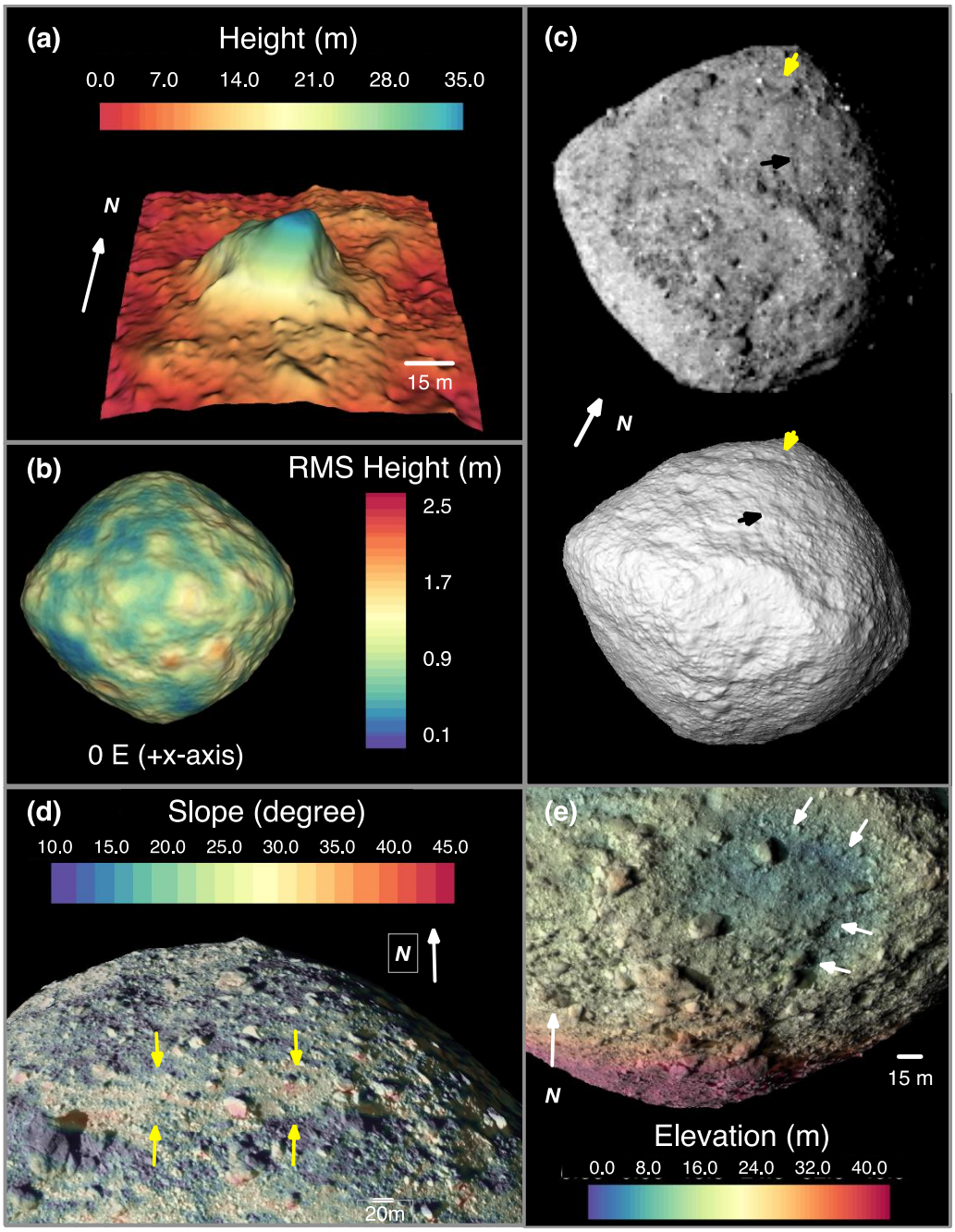

Figure 2: Geological features that contribute to the shape of Bennu. These include large boulders (a) such as the one located at -45S 132E that influence substantially the global roughness (b) measured as RMS Heights over horizontal scales of 10 m. Additional contributors to the shape include grooves (c: black arrows; top OCAMS image obtained Nov. 29, 2018 at 10:08:14 UTC) and scarps (c:yellow arrows and d; OCAMS image collected Dec. 12, 2018 at 7:12:28 UTC) as well as large craters (e) with landslide deposits (e: arrows; OCAMS image collected on Dec. 2, 2018 at 7:12:18 UTC).

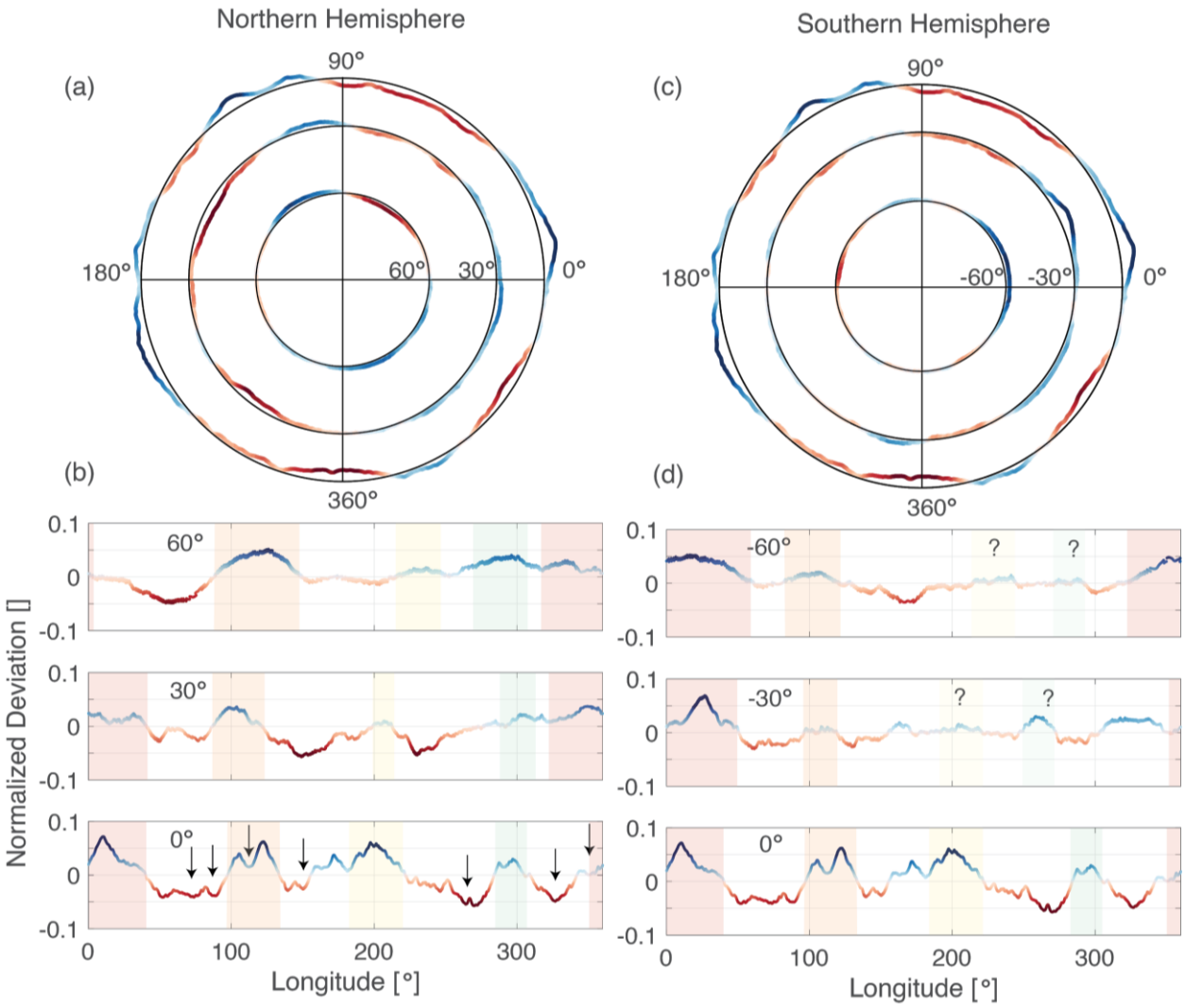

Figure 3: Deviations of Bennu's shape from a circle for different latitudinal cross-sections. [a] Best-fit circles for the shape of Bennu at 0°, 30°N, and 60°N overlain on Bennu's shape cross-sections and color-coded by deviations from the circle. [b] Deviations from the circular shape, normalized by the radius of the best-fit circles for 0°, 30°N, and 60°N. The shaded regions represent consistently elevated topography above the best-fit circles, interpreted as roughly North-South oriented ridges. At least two of them extend from the North to South polar regions. Arrows indicate locations of candidate craters [Walsh et al., this issue] that also contribute to the equatorial shape. [c] and [d] show similar plots for the southern hemisphere.

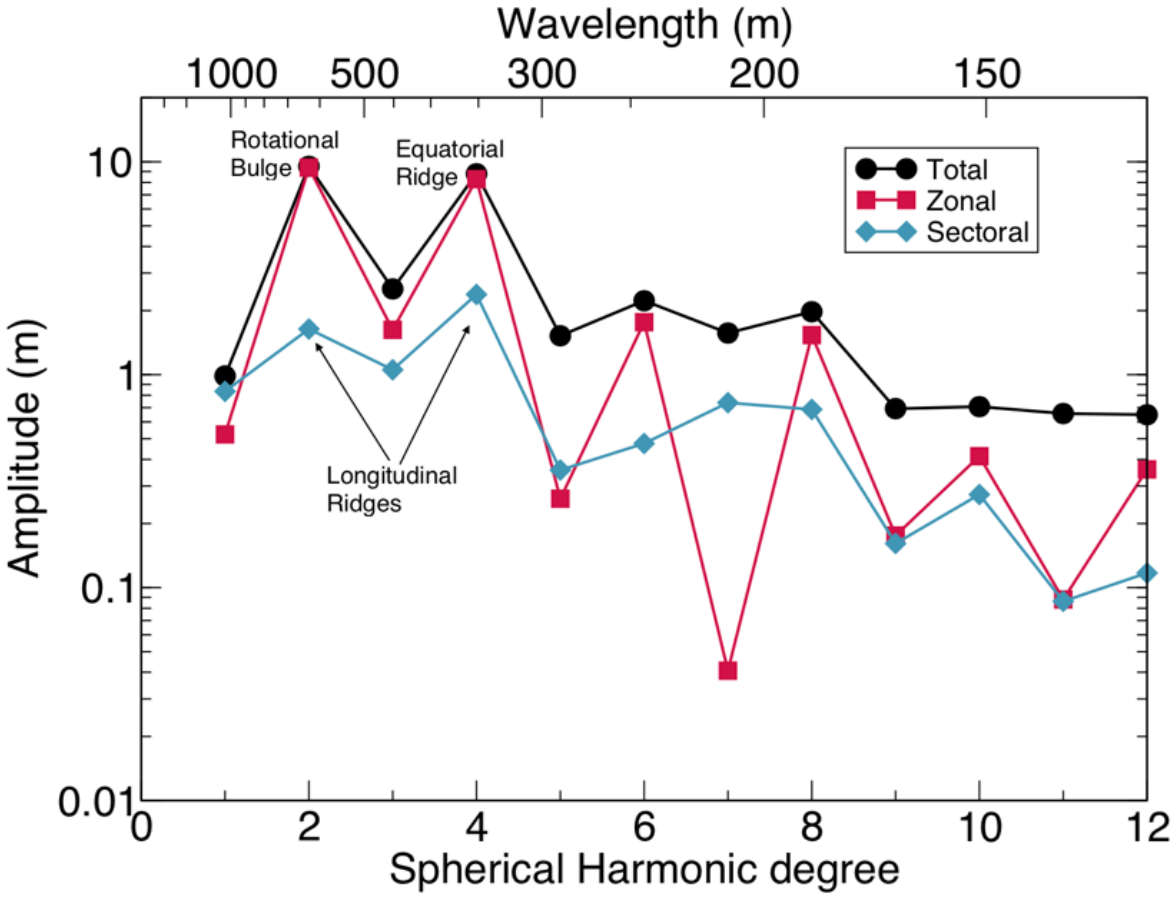

Figure 4: Amplitude spectrum of a spherical harmonic expansion for the shape model. Black dots indicate the total amplitude at each spherical harmonic degree *l*. Zonal terms (blue) describe contributions to the shape that vary only with latitude, sectoral contributions (red) vary only with longitude. The wavelength (given on top axis) is $2\pi R/l$, where *R* is the mean radius of Bennu. The large zonal degree-2 and -4 terms show the most distinctive characteristic of Bennu: the top shape with an equatorial ridge. Furthermore, the relatively low amplitudes of the degree 3 and 5 terms demonstrate that there is no substantial north-south asymmetry in Bennu's shape. The degree-4 sectoral terms (C_{44} and S_{44}), capture the ~ 90° longitudinal variations in shape associated with the major north-south ridges.

Method Section:

S1 Uncertainty of the Bennu shape model.

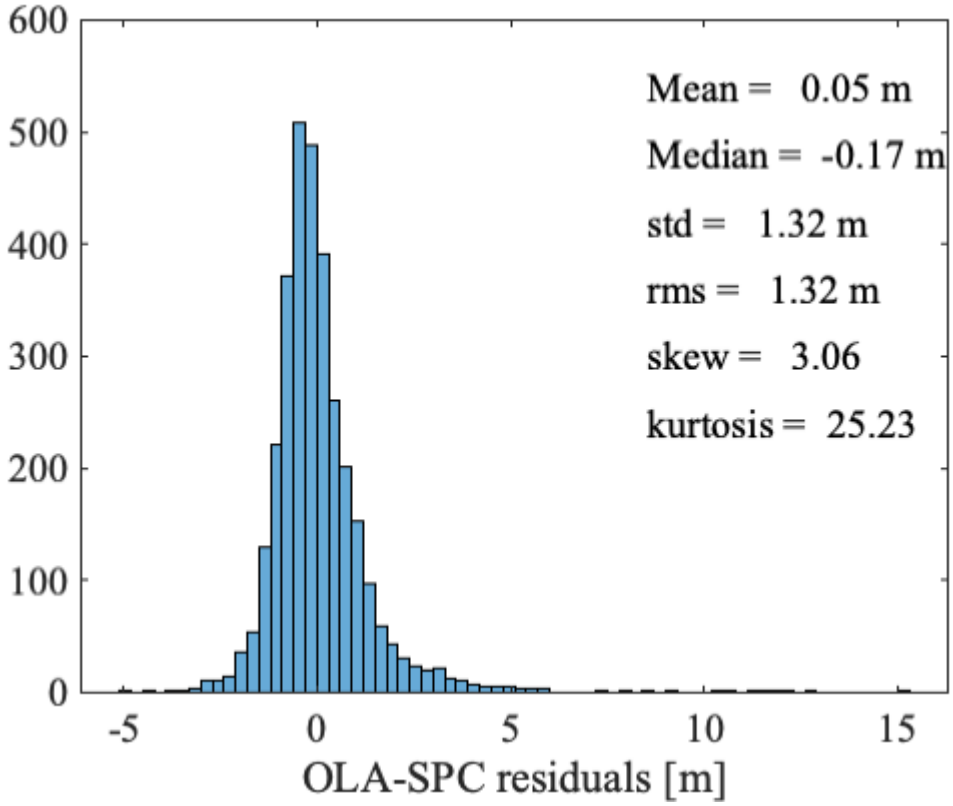

Figure S1A: OLA-based shape model evaluation: Residuals from comparing OLA returns with the SPC derived model. The median difference is ascribed as the uncertainty in the overall extent of the shape model, after the evaluation of a wide range of data, from limb information, to stereo derived vectors, and tracking of surface landmarks during the early stages of the orbital phase around Bennu. All the uncertainties measured are bound by the uncertainty obtained with OLA. (See Al Asad et al., 2019, Lunar and Planetary Science Conference for more details).

Section S2: Definition of the prime meridian.

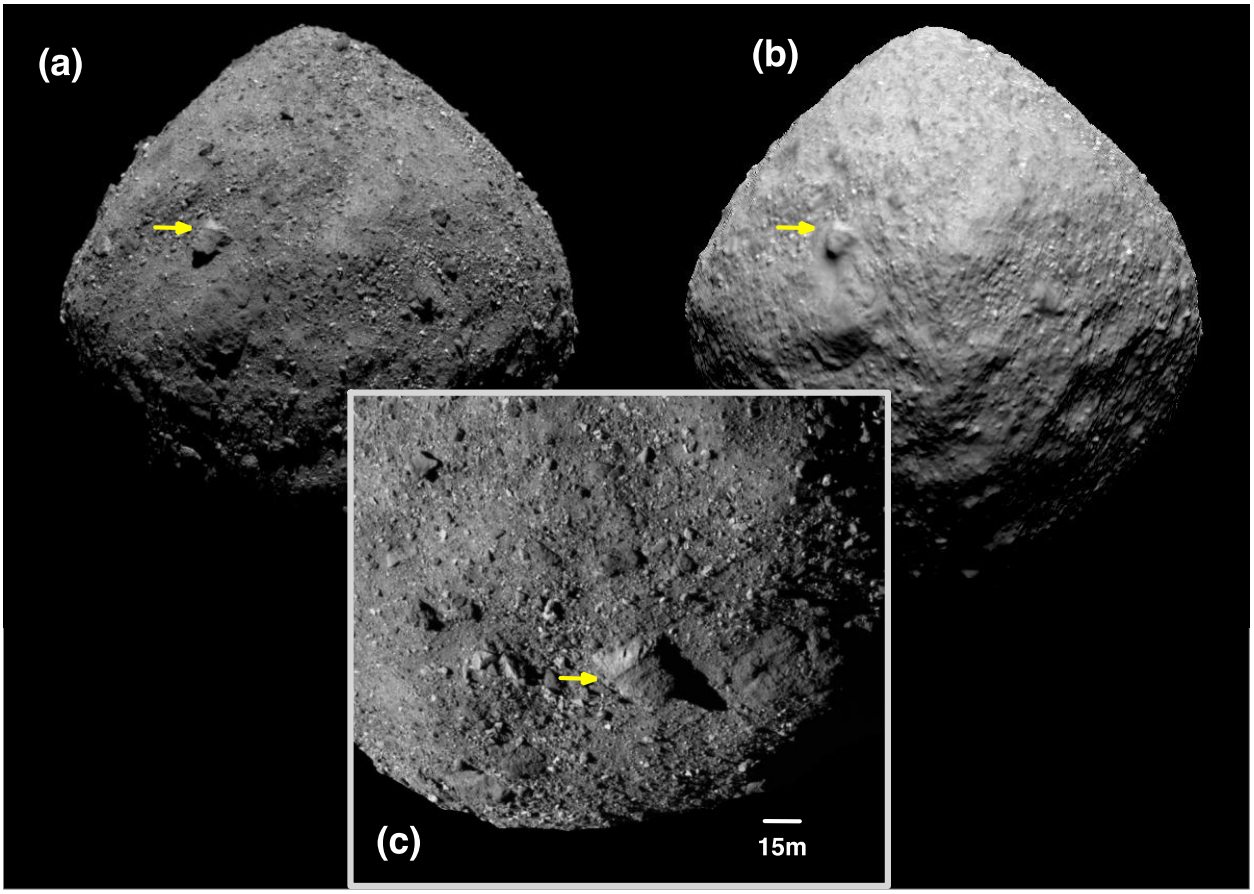

Figure S2A: The definition of the prime meridian for Bennu: The point indicated by the yellow arrows in the OCAMS images (a:collected on Nov. X, YYYY at ZZ UTC; c: Dec 2., 2018 at 6:07:44 UTC) and the Bennu global DTM (b) identify the location of the prime meridian identified by the OSIRIS-REx science team. It is shifted slightly by 1.6º of longitude from the current meridian defined in the Nolan et al. [1] radar model. This point is located at -28.5º latitude.

Section S3: The simplest model of rotating ellipsoidal figures in equilibrium is the Maclaurin spheroid; an oblate spheroid which arises when a fluid, self-gravitating body of uniform density ρ (a reasonable assumption for a small, rubble-pile asteroid [6]) rotates with constant angular velocity. This can be generalized to cohesionless solids [11]. The scaled spin is defined by:

$$\frac{\Omega^2}{\pi G\rho} = \frac{2\alpha\sqrt{m+2\alpha^2}}{m(1-\alpha^2)^{3/2}}\, cos^{-1}\,\alpha - \frac{2(m+2)\,\alpha^2}{m(1-\alpha^2)},$$

where *G* is the gravitational constant, *α* is the ratio of the polar (*c*) and equatorial (*a*) axes, and $m = (1 + sin\,\phi) / (1 - sin\,\phi)$, where φ is the angle of internal friction. A strengthless (i.e., fluid) body with no internal friction, would have *m* = 1; the Maclaurin formula. Alternative figures of equilibria exist. Jacobi ellipsoids for example, admit triaxial solutions [11, 21], although the distinction is unlikely to be significant for Bennu, and is more relevant to prolate asteroids (e.g., Eros or Itokawa).

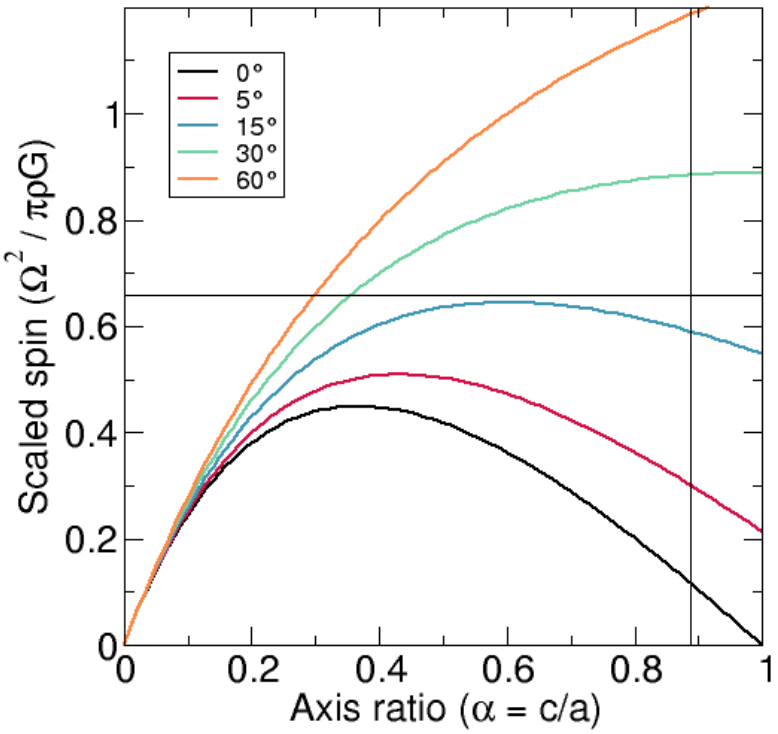

Figure S3A: Rotational stability for a cohesionless, solid, oblate spheroids for a wide range of rotation rate, oblateness, and internal friction: The curves of rotational stability for cohesionless, solid, oblate spheroids for a wide range of rotation rate, oblateness, and internal friction. Each curve describes the maximum dimensionless rotation rate as a function of . Any solution below the curve is stable. The horizontal line marks the scaled spin value consistent with the with the observed density (~1.2 g cm^{-3}) and rotation rate of Bennu (4.3 h) [6]; there are no stable solutions for a fluid body (lowermost curve). Some level of internal friction (or cohesion) is clearly necessary to prevent Bennu from further flattening, and undergoing either despinning or binary fission. For a spheroid with Bennu's and scaled spin parameter, satisfies the stability constraint.